Dinmohammadi et al. International Journal of Mechanical and Materials Engineering 2014, 9:24
http://www.springer.com/40712/content/9/1/24

International Journal of Mechanical and Materials Engineering
a SpringerOpen Journal

ORIGINAL ARTICLE Open Access

Water-based acrylic copolymer as an environment-friendly corrosion inhibitor onto carbon steel in 1 M H_2SO_4 in static and dynamic conditions

Hamid Reza Dinmohammadi[1], Ali Davoodi[2*], Gholam Ali Farzi[2] and Bahman Korojy[2]

Abstract

Background: The green corrosion inhibitors serve recently as a source of environmental friendly materials in the corrosive media. In present study, corrosion inhibitive performance of a new environment-friendly acrylic copolymer (methyl methacrylate/butyl acrylate/acrylic acid) on the mild steel in 1 M H_2SO_4 solution in the quiescence and hydrodynamic conditions was investigated.

Methods: Corrosion studies was performed by potentiodynamic polarization, electrochemical impedance Spectroscopy (EIS), quantum chemical calculations, optical microscopy and rotating disk electrode (RDE) techniques.

Results: Polarization experiment showed that the inhibition efficiency increased with increasing the inhibitor concentration and the inhibitor acted as mixed–type controls predominantly cathodic reaction in whole conditions. The thermodynamic calculations showed that the inhibitor obeys Langmuir adsorption isotherm. The increase in the inhibitor concentration and immersion time had a positive effect on inhibition efficiency while temperature had a negative effect. In the hydrodynamic conditions in 600 ppm (optimum inhibitor concentration), the most efficiency was at 1500 rpm rotation speed which was attributed to the enhance mass transfer of inhibitor to the metal surface and then decreased through the high shear stress. Theoretical Density function theory (DFT) calculations reveal that the unshared pairs of electrons on oxygen atoms in functional groups such as OH, C=O and also π electrons in double bonds in structures of three monomers are suitable centers to adsorb. Finally, optical images showed that the presence of inhibitor decreased the corrosion attack sites on the surface.

Conclusions: Acrylic copolymer (methyl methacrylate/butyl acrylate/acrylic acid was synthesized and it is suitable inhibitor for mild steel in 1M H_2SO_4 solution in static conditions and increasing its concentration increases its inhibition efficiency.

Keywords: Mild steel; Green copolymer; Acid corrosion inhibitors; EIS; Potentiodynamic polarization; Metallography

Background

In order to remove the undesirable scale and rust of metals, acidic solutions such as hydrochloric acid and sulfuric acid are the most common acids which are extensively used in the most industries, including chemical industries, petrochemical process, water cooling system, pickling system, boiler system, acid descaling industries, heat exchanger system, etc. (Schmitt 1984; Bentiss et al. 2007; Li et al. 2008; Abboud et al. 2006; Mernari et al. 1998; Singh et al. 1995; Muzaffer et al. 2008; Nable et al. 2008). Thus, in order to protect metal, using inhibitors for reduce the corrosion rate against the aggressive ions acid is one of the practical methods (Abd El-Maksoud and Fouda 2005; Wang 2001). Most of the well-known acid inhibitors are organic compounds containing nitrogen, oxygen and/or sulfur atoms, heterocyclic compounds, and π electron which cause improvement in the process inhibition efficiency (Liu et al. 2009; Ahamad et al. 2010; Foud and Ellithy 2009; Obot and Obi-Egbedi 2010; Soltani et al. 2010; Mahdavian and Ashhari 2010; Lowmunkong

* Correspondence: a.davoodi@hsu.ac.ir
[2]Materials and Polymer Engineering Department, Hakim Sabzevari University, Sabzevar 391, Iran
Full list of author information is available at the end of the article

et al. 2010; Kertit and Hammouti 1996). The inhibition efficiency of the inhibitors is substantially defined based on their adsorption properties. According to studies which carried out organic compounds, it has been reported that the adsorption of organic inhibitors mostly depends on some physiochemical properties of the molecule. The existence of functional groups in the organic inhibitors causes steric effects and electronic density of donor atoms. Adsorption also depends on the present double bonds having π electrons in the inhibitors that cause interaction between π orbitals of the inhibitor with vacant d orbitals of the surface metal atoms which induces greater adsorption of the inhibitor molecules on the surface of mild steel (Bentiss et al. 1999; Lukovits et al. 1995; Quraishi and Sharma 2002). Organic molecules could be adsorbed on the metal surface by one of the four following mechanisms: (a) electrostatic interaction between charged surface of the metal and the charge of the inhibitor, (b) interaction of unshared electron pairs in the inhibitor molecule with the metal, (c) interaction of π electron with the metal, and (d) a combination of the (a to c) types (Bentiss et al. 1999; Naderi et al. 2009). In recent years, some organic polymers were accepted as corrosion inhibitors which have environment-friendly characteristics and they have hydrocarbon chain length, less solubility, and also do not have toxic properties. Thus, the green inhibitors serve as a source which is environment-friendly in the inhibition corrosion process (Ali and Saeed 2001; Umoren and Open 2009). There are few studies in literatures about the inhibitor performance of organic and inorganic inhibitors on corrosion metals and alloys such as copper in the hydrodynamic conditions and also the effects of hydrodynamic conditions on the inhibitor performance under laminar or turbulent flow (Geler and Azambuja 2000). When the rotating speed is sufficiently high, rotating disk electrode (RDE) could also generate transition and relatively turbulent flows. The hydrodynamic effects such as flow velocity and shear stress at the surface influence fouling. The high shear stress causes separation of the protective layer from the metal surface, and also, it can influence the inhibition performance in the corrosion process (Jiang et al. 2005; Tian and Cheng 2008).

The objective of this study is to investigate the influence of solution in quiescence and hydrodynamic conditions on the corrosion behavior of st52 steel in 1 M H_2SO_4 solution in the absence and presence of copolymer acrylic (methyl methacrylate/butyl acrylate/acrylic acid). The presence of the copolymer is emulsified in aqueous solutions. This water-based copolymer was already used as an inhibitor in simulated sour petroleum solution in stagnant and hydrodynamic conditions, as an inhibitor in hydrochloric acid media, and also as an adhesive commercial resin in coating industry, and no scientific research has carried out on inhibitive performance of this copolymer as a corrosion inhibitor in sulfuric acid media so far. In this work, electrochemical methods including potentiodynamic polarization and electrochemical impedance spectroscopy (EIS) and quantum chemical calculations were used to model the structures of major constituents of the copolymer. These tests have been carried out in 0 (static), 500, 1,000, 1,500, and 2,000 (rpm) RDE in the absence and presence of 50, 200, 400, and 600 ppm inhibitor concentrations. The surface morphology of the polished mild steel in acid solution in the absence and presence of the inhibitor in the static and hydrodynamic conditions was investigated through optical microscopy imaging technique.

Experimental

Materials

Preparation of copolymer inhibitor The copolymer inhibitor was produced by using the free-radical addition copolymerization mechanism, and the molecular weight of this copolymer was 10^5 g/mol and the glass temperature was (Tg) about 20°C. The copolymer used in this work was a water-based acrylic terpolymer of methyl methacrylate/butyl acrylate/acrylic acid with 49/49/2 wt.% ratio, respectively, and with 50 wt.% water. Figure 1 shows the structures of three monomers with the presence of the copolymer.

Electrolyte

The invasive solution of 1 M H_2SO_4 was prepared by dilution of 98% H_2SO_4 (Merck, Whitehouse Station, NJ, USA) using distilled water. The concentration range of

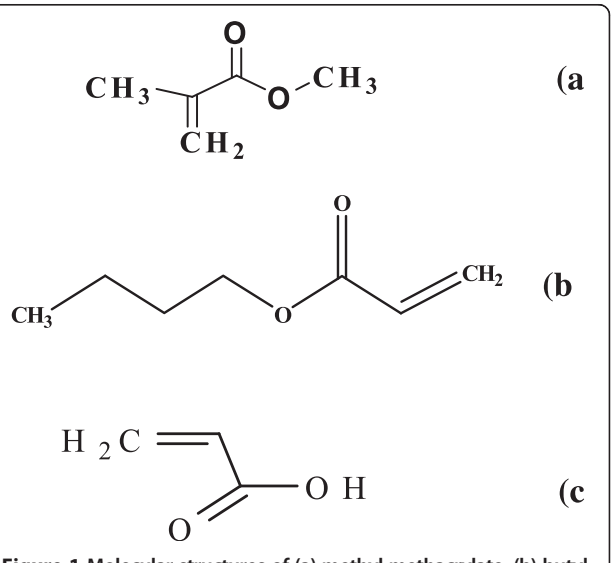

Figure 1 Molecular structures of (a) methyl methacrylate, (b) butyl acrylate, and (c) acrylic acid.

Table 1 Chemical composition of mild steel samples

Elements	C	Mn	Si	Cu	Cr	Ni	Mo	P	S
Wt.%	0.17	0.86	0.27	0.1	0.07	0.04	0.02	0.007	0.005

the copolymer employed was varied from 50 to 600 ppm concentration.

Preparation of specimen

The specimens of st52 steel rod with the following composition were presented in Table 1 (wt.% determined by quantum metric analysis); the remainder iron was used. The specimens were made by cold mounting of a rod mild steel sample with self-cure epoxy resin to expose a geometrical surface area of 0.45 cm^2 to the electrolyte. Before each experiment, the specimens (work electrode) were abraded with #60 to #1200 grades of emery papers and finally degreased with ethanol and washed in deionized water and then dried with flow of dry air.

Methods

Electrochemical measurements

Electrochemical experiments and corrosion tests were carried out using an IVIUM potentiostat (IVIUM Technologies, Fernandina Beach, FL, USA) connected to a computer through a USB cable and a conventional three-electrode cell. The cell was equipped with a steel electrode as the working electrode (WE), and the counter and reference electrodes were platinum wire and saturated calomel electrodes (SCE), respectively. In order to establish a steady state from open circuit potential (OCP), the working electrodes were first immersed into the test solution for 30 min. The potentiodynamic polarization curves were recorded at a scan rate of 1 mV/s in the potential range from −150 to +150 mV relative to the OCP. For linear polarization resistance measurement, the potential of the electrodes was scanned from −15 to +15 mV around OCP with 0.5 mV/s scan rate. The EIS measurements were performed at corrosion potentials over a frequency range of 100 KHz to 0.1 Hz with AC signal amplitude perturbation of ±10 mV. The electrochemical measurements in the hydrodynamic conditions were measured using an electrode controller (model: AFMSRCE, PINE Instruments Co., Durham, NC, USA) to control the rotation speed in the range (500 to 2,000 rpm) in the absence and presence of the inhibitor of various concentrations. EIS Analyzer Software was used to fit the experimental results of EIS measurements using appropriate equivalent circuit. Each measurement data point as shown in the figures and tables was performed at least three times, and reproducibility was satisfactory.

Quantum chemistry analysis

In order to ascertain about molecular structures of monomers, quantum chemical study was carried out. The molecular structures of monomers were drawn using the Gauss view 5.0. The optimized structures of the highest occupied molecular orbital (HOMO) and the lowest unoccupied molecular orbital (LUMO) of the three monomers were geometrically calculated by density functional theory (DFT) method using B3LYP level and 3-21G* basis set with Gaussian 98 software.

Optical microscopy

Optical microscopy was employed to investigate the effect of the inhibitor on the corrosion attack morphology in the absence and presence of the inhibitor. The specimen surfaces were mechanically polished down to 0.05 μm alumina slurry both in static and hydrodynamic conditions. The specimens were immersed in 1 M H_2SO_4 solution in the absence and presence of the inhibitor optimum concentration for 120 and 20 min in static and hydrodynamic conditions at room temperature, respectively. After bringing out from the solution, each specimen was washed and cleaned by ethanol and then dried with flow of dry air.

Results and discussion

Effect of inhibitor concentration

Potentiodynamic polarization study

Figure 2 shows polarization curves for the corrosion behavior of the mild steel in 1 M H_2SO_4 solution in the absence and presence of the inhibitor at 25 ± 2°C in quiescence conditions; some authors have mentioned that they cannot often accurately evaluate Tafel slopes by Tafel extrapolation because in the potentiodynamic polarization studies, the polarization curves do not display linear Tafel regions (Amin et al. 2009). Therefore, there

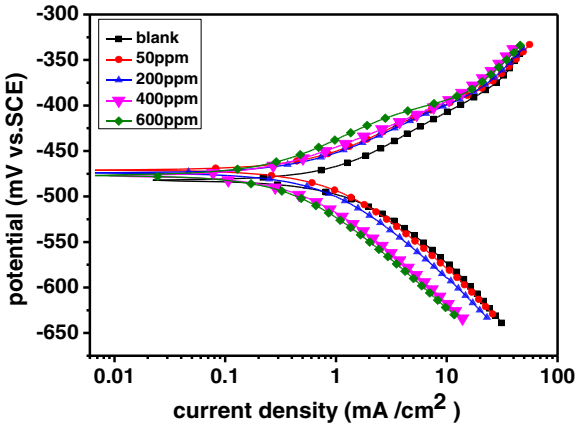

Figure 2 Polarization curves of mild steel in 1 M H2SO4 in different concentrations of the inhibitor in 25 ± 2°C.

are similar methods in software that can calculate the parameters of Tafel with acceptable deviation less than 10% from other methods of corrosion rate determination (Behpour et al. 2011). Electrochemical kinetic parameters such as corrosion potential (*E*corr), cathodic and anodic Tafel slopes (β_c and β_a), and corrosion current densities in the absence (i^0corr) and presence of the inhibitor (*i*corr) were extracted by Tafel extrapolating the anodic and cathodic lines and were listed in Table 1. The degree of surface coverage (θ) and the percentage of inhibition efficiency (η%) were calculated using the following equations (Qu et al. 2009):

$$\theta = \frac{i^0_{\text{corr}} - i_{\text{corr}}}{i^0_{\text{corr}}} \quad (1)$$

$$\%\eta = \theta \times 100 \quad (2)$$

With the inspection of the results in Table 2 and Figure 2, it can manifestly be explained that the current density values of mild steel in the presence of the inhibitor decreased in the range of 50 to 600 ppm concentrations. Consequently, this lead to the increase in the inhibition efficiency with the increase in the inhibitor concentration that indicates dependence of the corrosion current density on the inhibitor concentration. A maximum inhibition efficiency of about 76% was recorded for the copolymer at a concentration of 600 ppm, and with this, the concentration exhibited reverse effect to both the anodic process that refers to the iron dissolution reaction and the cathodic process that refers to the hydrogen evolution reaction of polarization curves, which have been decreased and are under activation and controlled in Figure 2, while the cathodic branch prominently decreased in comparison with the anodic branch. It can also be observed that the βa and βc values almost remain without change which indicates that the copolymer act as an adsorptive inhibitor. It reduces the anodic dissolution and also retards the hydrogen evolution reaction via blocking the active reaction sites without change in the corrosion mechanism of the metal dissolution and reduction of protons. The *E*corr values remain almost unchanged. Finally, it can be taken from the results that the copolymer acted as mixed-type inhibitor in 1 M H_2SO_4 solution (Abd El-Maksoud and Fouda 2005; Yan et al. 2008; Hasanov et al. 2010).

Electrochemical impedance spectroscopy study

The effect of the corrosion inhibitive behavior of mild steel in 1 M H_2SO_4 solution in the absence and presence of the inhibitor of various concentrations at 25 ± 2°C was presented in the form of Nyquist and Bode and phase angle plots in Figure 3a,b. From Figure 3a,b, it can be obviously seen that the impedance spectra shows a single depressed semicircle and the diameter of semicircle was increased with the increase in the inhibitor concentrations and only one time constant was observed in Bode format. In fact, an increase in the semicircle diameter indicates an increase in the corrosion resistance of mild steel in the presence of the inhibitor and also indicates one capacitive loop at high frequency (HF); the capacitive loop was attributed to the charge transfer that participates at electrode/solution interface of the corrosion process (Larabi et al. 2004; Li et al. 2010; Ashassi-sorkhabi et al. 2006). As it can be seen from Figure 3a, the semicircles were depressed into the *z*re (real axis) of Nyquist plot which is often attributed as frequency dispersion as a result of the inhomogeneity, roughness, impurities, dislocations, distribution of the active sites, adsorption of the inhibitors, and formation of porous layers on the mild steel surface (Noor 2009; Macdonald 1987). Thus, the capacitance is represented through a constant phase element (CPE) that is described in impedance representation as (Bommersbah et al. 2005; Benedetti et al. 1995):

$$Z_{\text{CPE}} = 1/Y_0(j\omega)^n \quad (3)$$

where Y_0 is the magnitude of the CPE, n is the CPE exponent ($-1 \le n \le 1$), ω is the angular frequency in rads^{-1} ($\omega = 2\pi f$ when f is the frequency in Hz), j is $(-1)1^{/}2$, and *Z*CPE is the impedance of CPE. Equivalent circuit used to fit the EIS data of mild steel was shown in Figure 4 which shows parallel combination of a charge transfer resistance (*R*ct) and constant phase element that is related to the capacity of the double layer (*C*dl). Both are in series with

Table 2 Polarization parameters and the corresponding inhibition efficiency of mild steel corrosion in 1 M H_2SO_4 containing different concentration of inhibitor at 25 ± 2°C

Concentration (ppm)	E_{corr} (mV vs. SCE)	i_{corr} (mAcm^{-2})	β_a (mV/dec)	β_c (mV/dec)	θ	η (%)
Blank	−482	0.606	101	102	-	-
50	−481	0.353	69	89	0.42	41.7
200	−474	0.255	64	81	0.58	57.7
400	−477	0.152	63	82	0. 75	74.8
600	−478	0.144	77	89	0.76	76.1

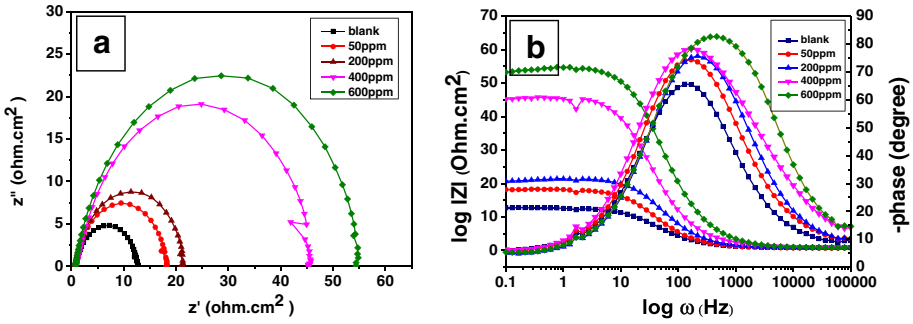

Figure 3 Typical (a) Nyquist (b) Bode magnitude and phase plots of mild steel in blank and inhibited solution in static conditions.

solution resistance (R_s). Therefore, the values of CPE capacitance were calculated by the following equation:

$$C_{\mathbf{dl}} = p^{1/n} \mathrm{R}_{ct}{}^{1-\mathbf{n}/n} \tag{4}$$

In the above expressions, p, n, and Rct are the magnitude of CPE, deviation parameter, and charge transfer resistance of mild steel, respectively. The fitted parameter values for various concentrations of the inhibitor were listed in Table 3. The results of this analysis show that Rct values increased, while Cdl values considerably diminished with the increase in the concentration of the copolymer. The increase in the Rct values represented the formation or reinforcement of a protective layer on the electrode surface, and this layer caused the barrier for mass transfer and charge transfer (Hirschorn et al. 2010; Bhpour et al. 2010). The values of double layer capacitance (Cdl) decreases by adding the inhibitor, and this indicates the gradual replacement of water molecule by the adsorption of the copolymer as a protective layer on the metal surface in the inhibited solution (Bentiss et al. 2000). In other words, the decrease in the Cdl value could be attributed to the decrease in local dielectric constant and/or an increase in the thickness of the electrical bouble layer (Sorkhabi et al. 2005). Thus, the thickness of this protective layer (δ) that is related to

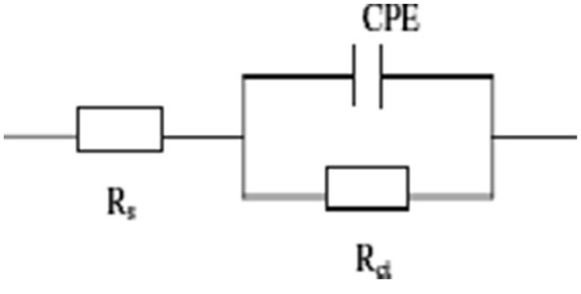

Figure 4 The electrochemical equivalent circuit for inhibited solution in static conditions.

Cdl according to Helmholtz model can be calculated by the following equation:

$$\mathrm{C_{dl}} = \frac{\varepsilon_O \varepsilon}{\delta} \mathrm{A} \tag{5}$$

where δ is the film thickness, ε is the dielectric constant of the medium, ε_0 is the vacuum permittivity, and A is the electrode area (Hamdy 2006; Boukamamp 1980). The inhibitor efficiency is calculated by using Equation 6 (Hamdy 2006):

$$\%\eta = \frac{R_{\mathrm{Ct}} - R^o{}_{\mathrm{Ct}}}{R_{\mathrm{Ct}}} \times 100 \tag{6}$$

where Roct and Rct are the charge transfer resistance values of mild steel in the absence and presence of the inhibitor, respectively. As is observed, the inhibitor efficiency value in optimum concentration 600 ppm by charge transfer resistance is in close correlation with those obtained from polarization results.

Polarization resistance study

The polarization resistance obtained values of mild steel in 1 M H_2SO_4 solution in the absence and presence of the inhibitor were listed in Table 3. Appraisal of Table 3 data shows that the R_p values were increased with the increase in the inhibitor concentrations; it can be explained that the adsorption of the inhibitor is effective, and it inhibits corrosion by blocking the active sites of the metal surface. As seen, the results of LPR confirm the inhibitive behavior of the copolymer, and it is in agreement with the results obtained from potentiodynamic polarization and EIS measurements.

Effect of immersion time

To investigate the effect of immersion times on the inhibitor behavior, EIS test was carried out in the presence of 600 ppm concentration of the inhibitor after 1-, 3-, 6-, and 9-h immersion at 25 ± 2°C (Figure 5). As known, EIS is an exact technique for long-term tests because it does not

Table 3 Electrochemical parameters of impedance for mild steel in 1 M H_2SO_4 solution in the inhibitor different concentrations at 25 ± 2°C in static conditions

Concentration (ppm)	EIS						LPR	
	R_s (ohm.cm^2)	R_{ct} (ohm.cm^2)	P (μFcm^{-2})	n	C_{dl} (μFcm^{-2})	η%	R_p (ohm.cm^2)	η%
Blank	0.89	11.9	860	0.89	1,085	-	65	-
50	0.79	17.38	540	0.89	731	32	89	27
200	0.85	21	410	0.85	506	43	103	37
400	1.3	45.5	290	0.88	378	74	220	70
600	1.4	54.4	130	0.88	377	78	258	75

considerably distract the system and it clearly indicates the experiment occurrences. As seen from Figure 5, the Nyquist plots for mild steel at various times are single capacitive loop that the diameters of the loops have increased with the increase in immersion times. The impedance parameters *R*ct, *R*S, and Cdl obtained from the EIS measurements were listed in Table 4. It should be noted that the *R*ct values increased and the *C*dl values decreased with the increase in immersion times. For the presence of 600 ppm copolymer concentration, the *R*ct value increased from 20 ohm.cm2 at 1 h to 38 ohm.cm2 at 9 h and the *C*dl value decreased from 1,038 μFcm⁻2 at 1 h to 144 μFcm⁻2 at 9 h. This means that the decrease in *C*dl is more probably due to the decrease in local dielectric constant and/or increase in the thickness of the electrical double layer that caused the formation of the protective layer at the electrode surface (Sorkhabi et al. 2005).

Effect of temperature

The activation energy of the metal corrosion process can be obtained by investigating and experimenting the effect of temperature on the corrosion inhibition behavior. Therefore, we can obtain some information about adsorption mechanism of the inhibitor by the activation energy values; for this purpose, the polarization test of mild steel in 1 M H_2SO_4 solution at different temperatures (25 ± 2°C to 50 ± 2°C) in the absence and presence of 600 ppm copolymer concentration was employed; see Figure 6a,b. As known, the temperature effect study in the corrosion process is very abstruse because when a reaction is carried out between an acid-inhibited solution and metal, many changes like rapid etching, desorption of the inhibitor, and inhibitor decomposition in the solution on the metal surface may occur (Bentiss et al. 2005). The electrochemical parameters were listed in Table 5. The evaluation of the Table 5 data shows which the corrosion current densities have increased in both the uninhibited and inhibited solutions with the increase in temperature, but the values of inhibition efficiency (η%) and also surface coverage (θ) was abruptly decreased at temperature 50 ± 2°C. It can be referred to diminish the strength of the adsorption process at elevated temperature and would also be suggested a physical adsorption mode (Herrag et al. 2010). Of course, it could be proposed to probably increase the decomposition of the copolymer at high temperatures. However, the current density of the mild steel inhibited is lower than the uninhibited mild steel in all temperatures. Thus, it can be said that the inhibition efficiency (η%) is dependent on the temperature in 1 M H_2SO_4 solution. The activation energy of the metal corrosion process according to the Arrhenius equation can be calculated using the following equation (7):

$$\ln i_{Corr} = \ln A\text{-}\frac{-Ea}{RT} \tag{7}$$

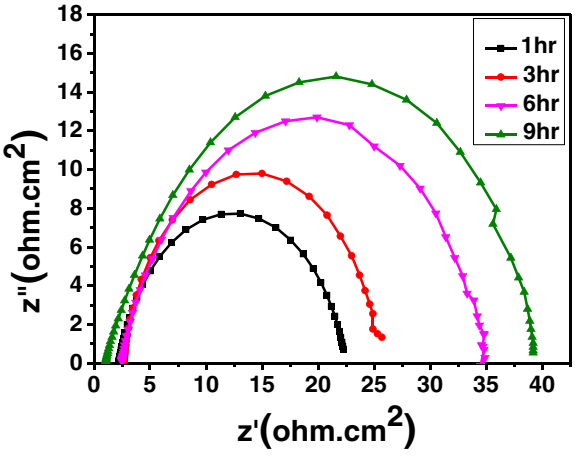

Figure 5 Effect of time on Nyquist plot of mild steel in inhibited solution in optimum concentration at 25 ± 2°C.

Table 4 Electrochemical parameters of impedance of mild steel in 1 M H_2SO_4 solution in time immersion conditions in the presence of optimum concentration of the inhibitor at 25 ± 2°C

Time (h)	R_{ct} (ohm.cm^2)	p (μFcm^{-2})	n	C_{dl} (μFcm^{-2})
1	20	2,000	0.83	1,038
3	22	500	0.85	225
6	33	400	0.85	186
9	38	300	0.86	144

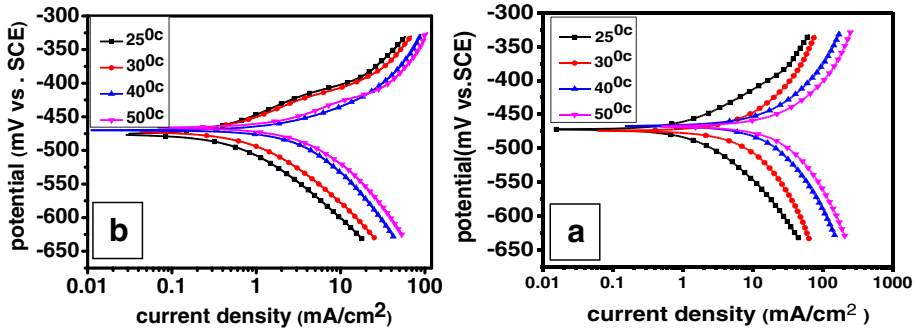

Figure 6 Effect of temperature on the potentiodynamic behavior of mild steel in (a) blank and (b) inhibited solutions in optimum concentration.

where E_a is the activation energy, A is the frequency factor, T is the absolute temperature, R is the gas constant, and i is the corrosion current density. By calculating the slope of ln($i$corr) vs. $1/T$ plot (Figure 7), the E_a value which is an indication of the adsorption mechanism will be obtained. The activation energy values relating to mild steel in 1 M H_2SO_4 solution in the absence and presence of the copolymer inhibitor have been listed in Table 6. As seen from Table 6, it is revealed that the value of Ea in the presence of the inhibitor is lower than that in the uninhibited solution, which can be attributed as chemical adsorption on the mild steel surface (Popova et al. 2003) and can also be attributed as slow rate of the inhibitor adsorption with a resultant closer approach to equilibrium during the experiments at high temperature (Hoar and Holliday 1953). Vračar and Dražić (2002) argued that the adsorption type obtained from the change of activation energy cannot be substantially taken as a basis as a decision through competitive adsorption with waters whose removal from the surface requires also some activation energy; in other words, the so-called chemisorption process may include simultaneous physical adsorption and vice versa.

Thermodynamic calculations of the inhibitor adsorption

There are several adsorption isotherms such as Langmuir, Temkin, Bockris-Swinkels, Flory-Huggins, and Framkin (Popova et al. 2003). For the study kinds of adsorption inhibitors, it can be used from the experimental data obtained in the polarization test. It could be fitted by Langmuir's adsorption isotherm. Thus, according to this isotherm, the value surface coverage (θ) is related to the inhibitor concentration (C) by the following equations (Bentiss et al. 2005):

$$\frac{\theta}{1-\theta} = K_{\text{ads}} C \tag{8}$$

Rearranging Equation 8 gives

$$\frac{C}{\theta} = \frac{1}{K_{\text{ads}}} + C \tag{9}$$

where K_{ads} is the equilibrium constant of inhibitor adsorption process which indicates the binding power of the inhibitor to the metal surface. C is the inhibitor concentration and θ is the surface coverage that was calculated by Equation 1. The plot of C/θ vs. C yields a

Table 5 Polarization parameters and the corresponding inhibition efficiency of mild steel corrosion in 1 M H_2SO_4 in the presence of optimum concentration of inhibitor at different temperatures

T (°C)	Solution	E_{corr} (mV vs. SCE)	I_{corr} (mAcm^{-2})	β_c (mV/dec)	β_a (mV/dec)	θ	η (%)
25	Blank	−482	0.606	102	101	0.22	22%
	Copolymer	−46	0.469	101	50		
30	Blank	−471	1.399	136	100	0.42	42%
	Copolymer	−467	0.793	104	54		
40	Blank	−468	4.279	141	106	0.70	70%
	Copolymer	−480	1.260	117	78		
50	Blank	−471	8.519	161	129	0.50	50%
	Copolymer	−469	4.187	134	83		

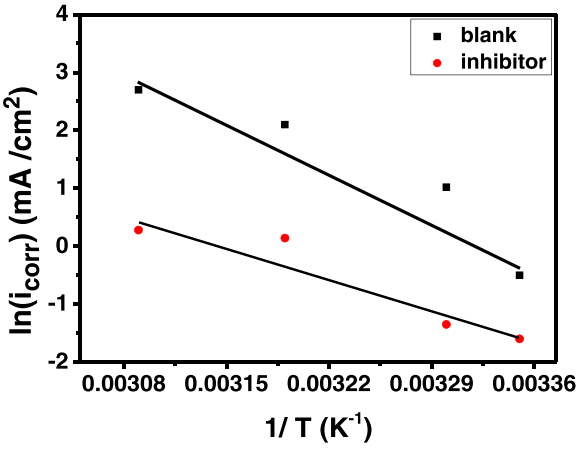

Figure 7 ln(*i*corr) vs. 1/*T* for mild steel dissolution in 1 M H2SO4 in the absence and presence of optimum concentration of the inhibitor.

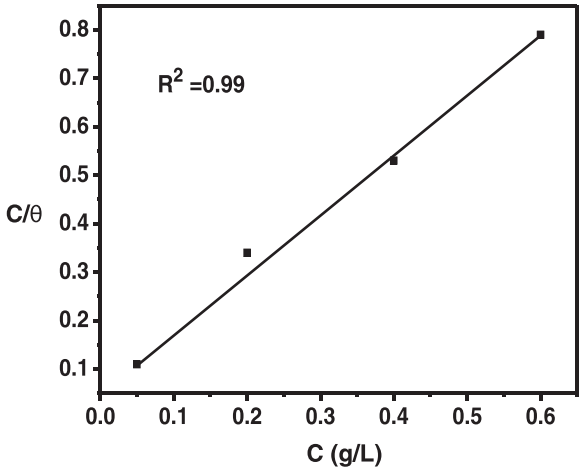

Figure 8 Langmuir adsorption isotherm of inhibitor in 1 M H2SO4 at 25 ± 2°C.

straight line as shown in Figure 8. The line regression coefficient (R^2) is almost equal to unity, and the slope is very close to unity. In fact, it represents that the adsorption of copolymer obeys the Langmuir adsorption isotherm. This means that the adsorbed inhibitor occupy only one site and do not interact with other adsorbed species (Avci 2008). K_{ads} value can be calculated from the intercepts of the straight line on the C/θ axis, which is related to the standard free energy of adsorption ΔG^0_{ads}, with the following equation (Khaled and AL-Qahtani 2009):

$$\Delta G^0_{ads} = -RT \ln(55.5 K_{ads}) \quad (10)$$

The value 55.5 in the above equation is the molar concentration of water in the solution in M (mol L^{-1}), R is the gas constant (8.314 kJ^{-1} mol^{-1}), and T is the absolute temperature (K). The ΔG^0_{ads} value is presented in Table 6. The negative sign of ΔG^0_{ads} is attributed to the adsorption of the inhibitor copolymer on the metal surface and the spontaneity of adsorption process (Avci 2008). The ΔG^0_{ads} value indicates the inhibitor function by physically adsorbing on the surface of the metal. Universally, values of ΔG^0_{ads} up to −20 kJ mol^{-1} are consistent with the electrostatic interactions between the charged inhibitor molecule and a charged metal that indicates physisorptions while values of ΔG^0_{ads} around or more than −40 kJ mol^{-1} indicate charge sharing or charge transfer from an organic molecule to the metal surface to form a coordinate type of metallic bond with the organic molecule that indicates chemisorptions (Solmaz et al. 2008). The heat adsorption (ΔH^0_{ads}) according to Gibbs-Helmholtz equation with good estimation can be calculated using Equation 11 (Avci 2008; Solmaz et al. 2008; Hosseini and Azimi 2009):

$$\ln \frac{\theta}{1-\theta} = \ln(B) + \ln(C) - \frac{\Delta H^0_{ads}}{RT} \quad (11)$$

where θ is the surface coverage, C is the inhibitor concentration, and B is a constant value plot of $\ln(\theta/1-\theta)$ vs. $1/T$ which yields a straight line as the slope and is shown in Figure 9 which is equal to $\Delta H^0_{ads}/20303R$, and also, the entropy of adsorption process (Δs^0_{ads}) can be

Table 6 Thermodynamic parameters for adsorption of inhibitor on mild steel surface in 1 M H_2SO_4 solutions

Solution	E_a kJ mol^{-1}	ΔG^o_{ads} kJ mol^{-1}	ΔH^o_{ads} kJ mol^{-1}	ΔS^o_{ads} J mol^{-1}
Blank	72.5	-	-	
Copolymer	62.4	−16.3	69	286

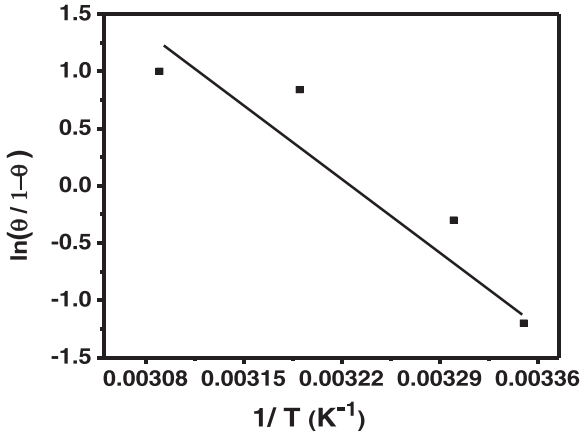

Figure 9 ln(θ/1 − θ) vs. 1/*T* for mild steel dissolution in 1 M H_2SO_4 in the presence of 600 PPM inhibitor.

calculated based on the following thermodynamic basic equation (Avci 2008; Bentiss et al. 2005):

$$\Delta G^0_{\text{ads}} = \Delta H^0_{\text{ads}} - T\Delta S^0_{\text{ads}} \quad (12)$$

ΔH^0_{ads} and ΔS^0_{ads} values are given in Table 6 by using Equations 11 and 12 which can calculate the values of thermodynamic parameters for the adsorption of inhibitor and also can obtain many information about the mechanism of corrosion inhibition. For instance, an endothermic adsorption process ($\Delta H^0_{\text{ads}} > 0$) is related to chemisorptions; an exothermic adsorption process ($\Delta H^0_{\text{ads}} < 0$) may be attributed to physisorptions, chemisorptions, or a mixture of both. In other words, in the enthalpy for the physisorptions process, it is less than 40 kJ mol^{-1}. Meanwhile, the enthalpy for the chemisorptions process is nearly 100 kJ mol^{-1} (Noor 2009; Bentiss et al. 2005). In this work, the value of ΔH^0_{ads} indicates chemisorption mechanism that is in agreement with the results obtained by the activation parameter (E_a) and, also, the value of ΔS^0_{ads} is larger than zero ($\Delta S^0_{\text{ads}} > 0$) which means that the process is a substitution process which can be related to the increase in water molecule desorption entropy (Solmaz et al. 2008; Li et al. 2009). It could also be interpreted with the increase of disorders due to the more water molecule which can be desorbed from the metal surface by one inhibitor molecule (Avci 2008; Solmaz et al. 2008).

Effect of hydrodynamic conditions

Potentiodynamic polarization study

The polarization curves of mild steel at the different rotating speeds in 1 M H_2SO_4 solution in the absence and presence of inhibitor are shown in Figure 10a,b. The polarization parameters including *i*corr, *E*corr, βa, and βc for blank and inhibited solutions in each rotation speed are given in Table 7. The values of inhibition efficiency η% are calculated using Equation 2. As can be observed from Figure 10a,b and also from Table 7 in the hydrodynamic conditions in the absence of the inhibitor case at various rotating speeds of the working electrode (500 to 2,000 rpm), the corrosion current density decreased and the *E*corr values slightly shifted toward more positive potential with the increase in the electrode rotation rate. It means that the electrode surface becomes nobler with the increase in the electrode rotation rate. It can probably be due to the presence of H^+ ions and dissolved oxygen which caused oxidation of the mild steel and formation of the oxide layers as protective layers on the electrode surface with the increase in the electrode rotating rate (Ashassi-Sorkhabi and Asghari 2008; Tian and Cheng 2008). In the presence of the inhibitor in 600 ppm optimum concentration, the corrosion current density considerably decreased until 1,500 rpm in the inhibited solution and then increased with the increase in the electrode rotation rate. The *E*corr values slightly shifted toward more positive potential with the increase in the electrode rotation rate. Therefore, it can be said that the copolymer acts as mixed-type inhibitor in 1 M H_2SO_4 solution as already said in quiescence conditions. As seen from Figure 10b, the cathodic corrosion current densities remarkably have decreased in comparison with the anodic corrosion current densities. In fact, the inhibitor indicating an inclination to more blocking the cathodic active sites which act as suitable for hydrogen evolution in hydrodynamic conditions (Noor 2009; Hirschorn et al. 2010; Khaled and AL-Qahtani 2009). It should be noted that although there is oxygen in the inhibited solution, the decrease in cathodic branch could not be referred to the oxygen reduction so that the oxygen reaches on the electrode surface until the process under the diffusion-controlled limit. In fact, it can be said that the inhibitor prevents hydrogen evolution reactions in the inhibited solution under activation-controlled inhibitor (Umoren et al. 2010). By the way, it is also revealed that cathodic curves in the polarization plots almost display a behavior of Tafel region, but the anodic polarization curves do not

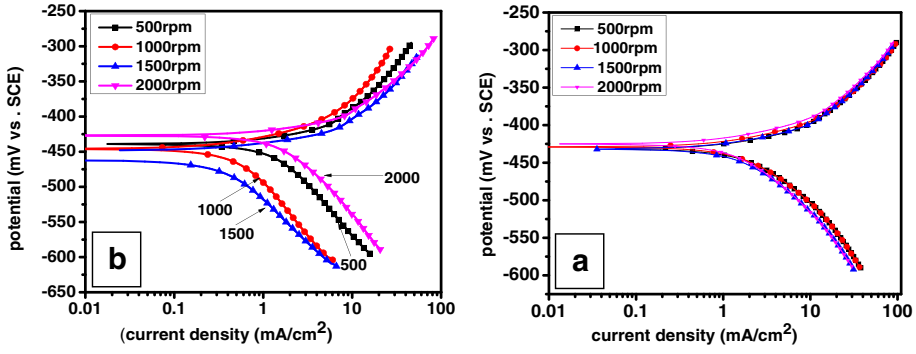

Figure 10 Typical polarization curves for corrosion of mild steel in the (a) blank (b) the presence of 600 ppm inhibitor in hydrodynamic conditions.

Table 7 Electrochemical potential polarization parameters for mild steel corrosion in the absence and presence of optimum concentration of inhibitor at different rotation speeds

Rotation speed (rpm)	Concentration (ppm)	E_{corr} (mV vs. SCE)	I_{corr} (mAcm^{-2})	β_C (mV/dec)	β_a (mV/dec)	θ	η (%)
500	Blank	−450	3.65	123	104	0.33	33
	600	−480	2.43	143	137		
1,000	Blank	−451	3.61	120	105	0.72	72
	600	−493	1.01	156	121		
1,500	blank	−458	3.24	120	107	0.84	84
	600	−481	0.512	125	78		
2,000	blank	−453	2.92	119	103	0.15	15
	600	−456	2.48	142	105		

display an extensive Tafel region, which may be due to the deposition of the corrosion products or impurities on the steel (e.g., Fe_3C) to form a non-passive surface film. The existence of deposition from corrosion products or impurities does not display as well as an anodic Tafel region which could cause deviations from Tafel behavior (Jones 1992; Khaled and Amin 2009). As known in the adsorption process of the inhibitor on the electrode surface, when a metal is immersed in an aqueous solution, the first step is when the water molecule covered on the metal surface must be displaced to the organic molecule inhibitor. The adsorption of organic molecule inhibitor from aqueous solutions is thus a replacement reaction (Borkris and Swinkels 1964).

$$\mathrm{Org}_{(\mathbf{soln})} + n\mathrm{H_2O}_{(\mathbf{ads})} \rightarrow \mathrm{Org}_{(\mathbf{ads})} + n\mathrm{H_2O}_{(\mathbf{Soln})} \quad (1)$$

The inhibitor may then combine with freshly generated Fe 2^+ ions on steel surface, forming metal inhibitor complexes (Oguzie et al. 2007; Branzoi et al. 2000).

$$\mathrm{Fe} \rightarrow \mathrm{Fe}^{2+} + 2e \quad (2a)$$

$$\mathrm{Fe}^{2+} + \mathrm{Inh} \rightarrow \left[\mathrm{Fe}^{2+} - \mathrm{Inh}\right]_{(\mathbf{ads})} \quad (2b)$$

As seen from Figure 10a, the maximum reduction of the corrosion current density and also the best and most efficient inhibition was 1,500 rpm with the increase in the electrode rotating speeds in the inhibited solution due to the enhancement in mass transfer of the inhibitor from bulk toward the metal surface. Thereafter, the corrosion current density increased and the values of inhibition efficiency decreased in the rate 2,000 rpm. In this investigation, it can be explained that in higher velocities of flow probably through interference, the high shear stress causes separation and dislodgement of the inhibitor layers or adsorbed [Fe2$^+$-Inh] complex from the metal surface and can result to the decrease in the value of the inhibition efficiency with the increase in the electrode rotating speeds (Jiang et al. 2005). However, hydrodynamic conditions may have beneficial or harmful effects in the values of the inhibition efficiency. Therefore, as mentioned in the literature, in hydrodynamic flow conditions, there are many different effects on the inhibition performance (Jiang et al. 2005):

(i.) In the hydrodynamic conditions, the flow can increase mass transport of inhibitor molecules that causes more inhibitor presence at the metal surface. This effect can improve the inhibitor performance.
(ii.) Hydrodynamic conditions can increase mass transport of metal ions (Fe^{2+}), produced during metal dissolution from electrode surface to the bulk of solution and hence lead to less [Fe2$^+$-Inh] complex in the presence of the electrode; this is a harmful effect for inhibition performance.
(iii.) The high shear stress resulted from high flow velocity can also separate inhibitor layer or adsorbed [Fe2$^+$-Inh] complex and cause more desorption from the metal surface which acts as a negative factor on inhibition efficiency.

The balance of the abovementioned effects lead to changes in the surface coverage, θ, and inhibition efficiency (η%) with rotation speed.

Electrochemical impedance spectroscopy study

Figure 11a,b shows Nyquist plots of mild steel in 1 M H_2SO_4 solution at various rotation speeds in the absence and presence of inhibitor in 600 ppm optimum concentration. In the blank case, the impedance spectra exhibits one single depressed semicircle and the diameter of semicircle increases with the increase of the electrode rotation rate which attributed to the oxidization reaction of the mild steel and formation of the oxide film as a protective layer on the metal surface due to the presence of H^+ ions and dissolved oxygen in the uninhibited solution (Ashassi-Sorkhabi and Asghari 2008; Tian and Cheng 2008). This trend confirms that the results of the uninhibited solution were obtained from polarization measurements. As is observed from Figure 11b, the

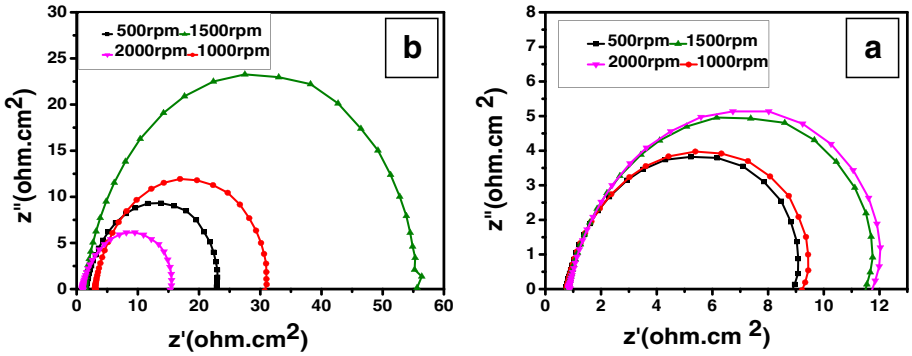

Figure 11 Typical Nyquist plots obtained for mild steel in hydrodynamic conditions in (a) blank and (b) inhibited solution in optimum concentration.

diameter of semicircles has been increased to 1,500 rpm since they have been reduced with the increase in the electrode rotating rate. In other words, it had the reverse effect at the higher velocities than 1,500 rpm in the inhibited solution. As described in section the 'Potentiodynamic polarization study', there are many factors which affect the behavior of the inhibitor in high flow velocity. On the one hand, it can improve the performance of the inhibitor through the increase of inhibitor mass transfer form bulk toward the metal surface; on the other hand, at higher speeds through interference, the high shear stress causes separation of the inhibitor layers or adsorbed [$Fe2^{+}$-Inh] complex from the metal surface (Jiang et al. 2005). The balance of the abovementioned expressions can result to changes of the inhibition efficiency (η%) and surface coverage (θ) with the increase in the electrode rotation rate. An appropriate equivalent circuit for inhibited solution in hydrodynamic conditions is similar to the equivalent circuit in static conditions (Figure 4) where R_S is the solution resistance, RCt is the electron transfer resistance, and CPE is the constant phase element (which increases from the time constant of the electrical double layer). The values of Cdl have been calculated using Equation 4. CPE was generally used in the model to compensate for the inhomogeneities in the electrode surface as depicted by the depressed nature of the Nyquist semicircle (Nyikos and Pajkossy 1985). The results obtained from the impedance parameters were analyzed by EIS Analyzer Software from EIS plots. These results were shown in Table 8. It can be explained that the maximum value RCt and also the most efficient inhibition is at 1,500 rpm in the inhibited solution that is attributed to enhance the mass transfer of the inhibitor from the bulk solution toward the metal surface (Jiang et al. 2005). Thereafter 2,000 rpm, the values RCt reduced through the high shear stress that causes separation of the inhibitor protective layers from the metal surface. It is even observed that the RCt value at 2,000 rpm from the abovementioned expression becomes much less than 500 rpm in the inhibited solution.

Corrosion attack morphology study

Quantum chemical study

Quantum chemical methods are very useful in determining the molecular structure and also can explained about the electronic structures and reactivity of the molecule (Kraka and Cremer 2000). Geometric structure and electronic properties of the copolymer monomers were calculated by DFT method by using B_3LYP level and 3-21G* basis set with Gaussian 98 software. The optimized

Table 8 Electrochemical parameters of impedance for mild steel corrosion in absence and presence of optimum concentration of inhibitor at different rotation speeds

Rotation speed (rpm)	Concentration (ppm)	R_s (ohm.cm^2)	R_{ct} (ohm.cm^2)	p (μFcm^{-2})	n	C_{dl} (μFcm^{-2})	θ	η %
500	Blank	0.91	8.7	600	0.92	380	0.61	61
	600	1.9	22	200	0.89	102		
1,000	Blank	1	8.9	500	0.93	333	0.70	70
	600	3.3	30	171	0.89	89		
1,500	Blank	1.2	11	400	0.95	301	0.80	80
	600	1.8	55	112	0.90	64		
2,000	Blank	1.3	11.4	300	0.96	337	0.24	24
	600	1.1	15.1	300	0.87	134		

monomers structure of the copolymer and the frontier molecule orbital density distribution of the studied copolymer monomers are shown in Figure 12. The quantum chemical parameters calculated such as *E*HOMO (the energy of the highest occupied molecular orbital), *E*LUMO (the energy of the lowest unoccupied molecular orbital), ΔE (energy gap), and μ (dipole moment) are listed in Table 9. It has been reported in the literature that the higher HOMO energy of the inhibitor, the greater the trend of offering electrons to unoccupied d orbital of the metal and the higher the corrosion inhibition efficiency. In addition, the lower LUMO energy, the easier acceptance of electrons from metal surface, as the energy gap (ΔE = *E*LUMO – *E*HOMO) decreased and the value efficiency of inhibitor improved (Musa et al. 2010). It is generally accepted that for organic compound with lower LUMO, greater adsorption ability and better corrosion inhibition are expected (Herrag et al. 2010). It has also been reported that excellent inhibition corrosion properties are usually obtained using organic compounds that not only offer electrons to unoccupied orbitals of the metal but also accept free electrons from the metal by using their anti-bond orbitals to form stable chelates (feedback bond) (Herrag et al. 2010; Fang and Li 2002). In fact, the LUMO orbital can accept the electrons in the d orbital of the metal using anti-bonding orbitals to form a feedback bond. Thus, by forming feedback bonds, the chemical adsorption of inhibitor molecule on the steel surface increases and the inhibition efficiency also increases (Herrag et al. 2010). As it can be seen from Figure 12, there are dense regions that indicate greater adsorption of copolymer monomers on the mild steel surface. It is clear that among the HOMO and LUMO orbitals in the constituents of the copolymer, the electronic density were localized around the C = C double bonds and O atoms in -OH groups and also C = O groups. As known, the type of bonding electrons in C = C is π bonding electrons while for O atoms, hydroxyl and carbonyl groups are non-bonding pair. It can be suggested that the π electrons in (CH2 = CH) vynil group and unshared pair of electrons on oxygen atoms of carbonyl groups and also hydroxyl groups are suitable sites which would lead to greater adsorption of the inhibitor on the surface of the mild steel. The obtained result of the quantum chemical calculations indicates higher *E*HOMO and lower dipole moment (μ) values for butylacrylate monomers. Therefore, this represent a strong anti-bond to form stable chelates (feedback bond) and lead to greater adsorption with the metal protected from the corrosion in acid media (Herrag et al. 2010). Furthermore, it can also be observed manifestly the difference between the HOMO orbital and LUMO orbital of butyl acrylate monomers due to the fact that a typical geometry configuration of the monomer in the HOMO orbital electronic density is distributed in the greater portion of monomer surface with respect to the LUMO orbital; this means that the monomers have greater trend to donate electrons to the unoccupied d orbital of the metal. Consequently, it is noticeable that the inhibitor studied in this work acts on the basis of acceptance and donor of unshared pair of π electron clouds on the vynil group with unoccupied d orbital of the mild steel. The authors are not unanimous about the influence of the dipole moment on corrosion inhibition. Some authors showed that an increase of the dipole moment leads to the decrease of inhibition and vice versa, suggesting that lower values of the dipole moment will favor accumulation of the inhibitor in the surface layer. In

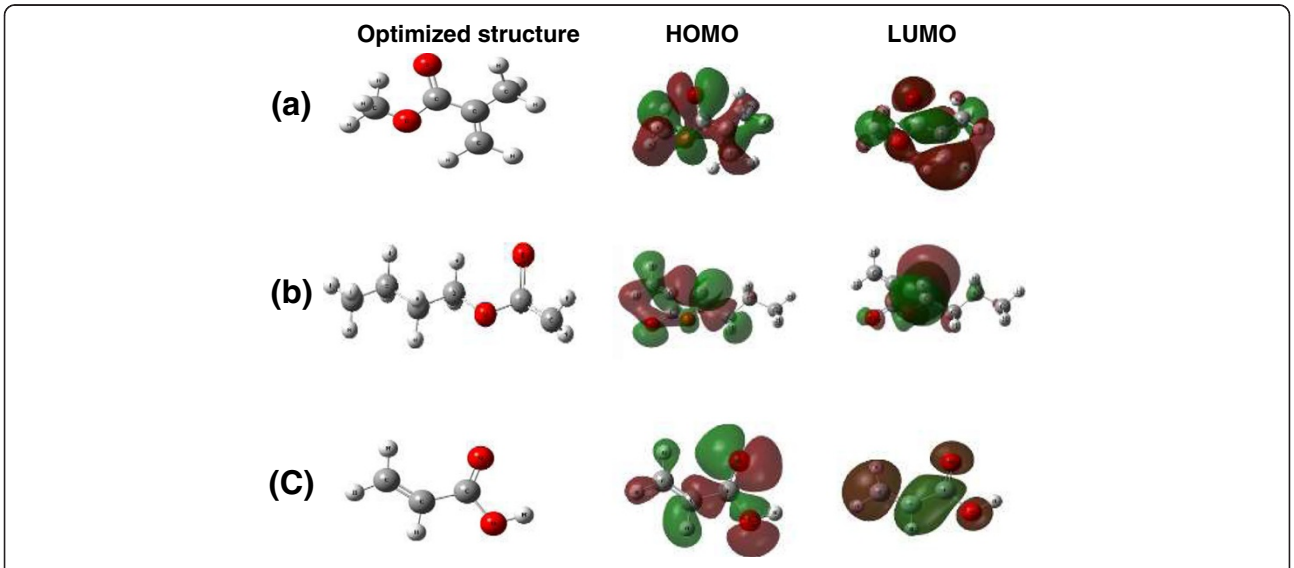

Figure 12 Molecular structure, molecular orbital plots of monomers of copolymer (a) methyl methacrylate, (b) butyl acrylate, and (c) acrylic acid.

Table 9 Quantum chemical parameters of monomers calculated by DFT method

Monomer	E_{HOMO} (ev)	E_{LUMO} (ev)	ΔE (ev)	μ (debye)
Methyl methacrylate	−0.2920	−0.0499	0.2420	2.640
Butyl acrylate	−0.2527	0.0422	0.2950	2.003
Acrylic acid	−0.2551	−0.0213	0.2764	2.209

contrast, the increase of dipole moment can lead to the increase of the inhibition and vice versa which could be related to the dipole-dipole interaction of the molecules and metal surface (Oguzie et al. 2010). Thus, it can be suggested that by the increase in the weight percentage of methyl methacrylate monomer and butyl acrylate, the adsorption of the inhibitor will increase onto the mild steel surface and, consequently, the inhibition efficiency will increase, too.

Optical microscope

Corrosion attack morphologies of the mild steel specimens in the absence and presence of the inhibitor for 120 and 20 min immersion in static and hydrodynamic conditions, respectively, have been investigated by optical microscopy and exhibited in Figure 13. As can be observed from Figure 13, the polished surface of specimen immersed in uninhibited solution has been corroded and was rough, but at the same time, the specimen in the presence of the inhibitor solution is remarkably covered with a protective layer of the inhibitor. Although a number of pits is observed on the mild steel surface due to the attack of the corrosive solution in static conditions in the hydrodynamic conditions 2,000 rpm, the specimen immersed in the uninhibited solution shows that grain boundaries has been severely corroded and a black appearance due to strong corrosion by corrosive solution is also observed. Therefore, it can be observed that the specimen structure has been more demolished in comparison with the inhibited specimen one.

Conclusions

1. Copolymer acrylic (methyl methacrylate/butyl acrylate/acrylic acid) was synthesized, and it is a suitable inhibitor for mild steel in 1 M H_2SO_4 solution in static conditions, and increasing its concentration increases its inhibition efficiency.
2. Potentiodynamic polarization studies showed that the inhibitor act as a mixed-type inhibitor.
3. The results of EIS on mild steel in the solution containing the inhibitor in static conditions showed that the charge transfer resistance increases and the surface capacitance decreases. This is indeed an indication of inhibitor adsorption onto the mild steel surface.
4. The adsorption of the inhibitor obeys Langmuir's adsorption isotherm, and thermodynamic data extracted showed both anodic and cathodic adsorption.
5. The results of polarization and EIS measurements for mild steel in the inhibited solution in hydrodynamic conditions showed that maximum inhibition efficiency was at 1,500 rpm electrode rotation rate that could be attributed to enhance mass transfer of inhibitor species from the bulk solution to the metal surface. Beyond 2,000 rpm, the

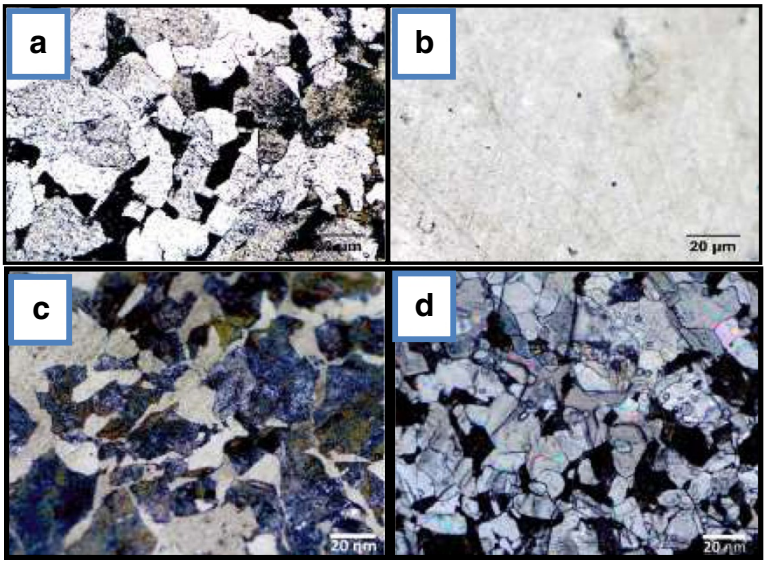

Figure 13 Optical microscopy images. (a) Blank solution in static conditions, **(b)** inhibited solution in static conditions, **(c)** blank solution in hydrodynamic conditions, and **(d)** inhibited solution in hydrodynamic conditions (2,000 rpm).

inhibition efficiency decreased that could be attributed to interference of the high shear stress which causes separation and dislodgement of the inhibitor protective layers from the metal surface.

6. Quantum chemical calculations of *E*HOMO and *E*LUMO showed that the *E*HOMO for butyl acrylate is higher than other monomers and *E*LUMO for methyl methacrylate is lower than other monomers. It also revealed that C = C double bond and unshared pair of electrons on O in C = O group and -OH group could be suitable centers for adsorption on the metal surface.
7. Optical microscopy obviously showed that there are severe corrosion and roughness on the surface of metal in the absence of inhibitor both in static and hydrodynamic conditions compared with those in the inhibited solutions.

Competing interests
The authors declare that they have no competing interests.

Authors' contributions
HRD performed all experiments as MSc student, analyzed the whole extracted data and plotted them, performed theoretical calculation and wrote the first draft of manuscript. AD initiated the idea as main supervisor and corresponding author, contributed in theoretical and experimental data analysis and interpretation, corrected and finalized the manuscript and replied to the comments. GAF performed copolymer synthesis, general discussion on solution preparation as second supervisor and contributed in final paper corrections on polymer section. BK contributed in used steel microstructure characterization, metallographic examination and final paper corrections on that part.

Acknowledgements
The authors appreciate the Materials and Metallurgical Engineering Department, Faculty of Engineering, Khorasan Razavi, Neyshabur; Science and Research branch, Islamic Azad University, Neyshabur, Iran; Materials and Polymers Engineering Department, Hakim Sabzevari University; and Sabzevar University for providing the organic compound used in this research and laboratory facilities during this study.

Author details
[1]Material and Metallurgical Engineering Department, Faculty of Engineering, Khorasan Razavi, Neyshabur, Science and Research branch, Islamic Azad University, Neyshabur, Iran. [2]Materials and Polymer Engineering Department, Hakim Sabzevari University, Sabzevar 391, Iran.

Received: 23 April 2014 Accepted: 27 October 2014
Published online: 21 November 2014

References
Abboud, Y, Abourriche, A, Saffaj, T, Berrada, M, Charrouf, M, Bennamara, A, Cherqaoui, A, & Takky, D. (2006). APPL. *Surf.* Science , *252*, 8178–8184.
Abd El-Maksoud, SA, & Fouda, AS. (2005). Materials chemistry and physics. *93*, 84–90.
Ahamad, I, Prasad, R, & Quraishi, MA. (2010). *Corrosion Science., 52*, 933–942.
Ali, SA, & Saeed, MT. (2001). *Polymer, 42*, 2785–2794.
Amin, MA, Abd EL-Rehim, SS, El-Sherbini, EEF, Hazzazi, OA, & Abbas, MN. (2009). *Corrosion Science, 51*, 658–667.
Ashassi-Sorkhabi, H, & Asghari, E. (2008). *Electrochmi Acta, 54*, 162–167.
Ashassi-sorkhabi, H, Ghalebsaz-Jeddi, N, Hashemzadeh, F, & Jahani, H. (2006). *Electrochim Acta, 51*, 3848.
Avci, G. (2008). *Colloid Surf A, 317*, 730–736.
Behpour, M, Ghoreishi, SM, Khayatkashani, M, & Soltani, N. (2011). *Corrosion Science, 53*, 2489–2501.
Benedetti, AV, Sumodjo, PTA, & Nobe, K. (1995). *Electrochim Acta, 40*, 2657.
Bentiss, F, Legrenée, M, Traisnel, M, & Hornez, JC. (1999). *Corrosion Science, 41*, 789–803.
Bentiss, F, Traisnel, M, & Legrenée, M. (2000). *Corrosion Science, 42*, 127.
Bentiss, F, Lebrini, M, & Legrenée, M. (2005). *Corrosion Science, 47*, 2915–2931.
Bentiss, F, Bouanis, M, Mernari, B, Traisnel, M, Vezin, H, & Lagrenée, M. (2007). *Applied Surface Science, 253*, 3696.
Bhpour, M, Ghoreishi, SM, Mohammadi, N, Soltani, N, & Salavati-Niasari. (2010). *Corrosion Science, 52*, 4046–4057.
Bommersbah, P, Alemany-Dumont, C, PMillet, J, & Normand, B. (2005). *Electrochim Acta, 51*, 1076–1084.
Borkris, JOM, & Swinkels, DAJ. (1964). *Journal of the Electrochemical Society, 111*, 736.
Boukamamp, BA. (1980). *Solid State Lonics, 20*, 31.
Branzoi, V, Branzoi, F, & Baibarac, M. (2000). *Materials Chemistry and Physics, 65*, 288.
Fang, J, & Li, J. (2002). *Journal of Molecular Structure, 593*(THEOCHEM), 179.
Foud, AS, & Ellithy, AS. (2009). *Corrosion Science, 51*, 868–875.
Geler, E, & Azambuja, DS. (2000). *Corrosion Science, 42*, 631–643.
Hamdy, H. (2006). *Electrochim Acta, 51*, 5966–5972.
Hasanov, R, Bilge, S, BilgiÇ, S, Gece, G, & KihÇ, Z. (2010). *Corrosion Science, 52*, 984–990.
Herrag, L, Hammati, B, Elkadiri, S, Aouniti, A, Jama, C, Vezin, H, & Bentiss, F. (2010). *Corrosion Science, 52*, 3042–3051.
Hirschorn, B, Orazem, ME, Tribollet, B, Vivier, V, Frateur, I, & Musiani, M. (2010). *Electrochim Acta, 55*, 6218–6227.
Hoar, TP, & Holliday, RD. (1953). *Journal of Applied Electrochemistry, 3*, 502.
Hosseini, SMA, & Azimi, A. (2009). *Corrosion Science, 51*, 620728–732.
Jiang, X, Zheng, YG, & Ke, W. (2005). *Corrosion Science, 47*(11), 2636.
Jones, DA. (1992). *Macmillan*. New York.
Kertit, S, & Hammouti, B. (1996). *Applied Surface Science, 93*, 59.
Khaled, KF, & AL-Qahtani, MM. (2009). *Mate Chem Phys, 113*, 150–158.
Khaled, KF, & Amin, MA. (2009). *Corrosion Science, 51*, 1964–1975.
Kraka, E, & Cremer, D. (2000). *Journal of the American Chemical Society, 122*, 8245–8264.
Larabi, L, Harek, Y, Traisnel, M, & Mansri, A. (2004). *Journal of Applied Electrochemistry, 34*, 833–839.
Li, X, Deng, S, Mu, G, Fu, H, & Yang, F. (2008). *Corrosion Science, 50*, 420.
Li, X, Deng, S, Hui, F, & Guannan, M. (2009). *Corrosion Science, 51*, 620–634.
Li, X, Deng, S, & Fu, H. (2010). *Corrosion Science, 52*, 2786–2792.
Liu, S, Xu, N, Duan, J, Zeng, Z, & Feng, Z. (2009). *R. Xiao. Corrosion Science, 51*, 1356–1363.
Lowmunkong, P, Ungthararak, D, & Sutthivaiyakit, P. (2010). *Corrosion Science, 52*, 30–36.
Lukovits, I, Kalman, E, & Palinkas, G. (1995). *Corrosion, 51*, 201.
Macdonald, JR. (1987). *Journal of Electroanalytical Chemistry, 223*, 25–50.
Mahdavian, M, & Ashhari, S. (2010). *Electrochim Acta, 55*, 1720–1724.
Mernari, B, Elattari, H, Traisnel, M, Bentiss, F, & Legrenée, M. (1998). *Corrosion Science, 40*, 391.
Musa, AY, Kadhum, AAH, Mohamad, AB, Rahoma, AAB, & Mesmari, H. (2010). *Journal Mol Strct, 969*, 233–237.
Muzaffer, Z, Ramazan, S, & Gülfeza, K. (2008). *Phyicochem Eng Aspect, 33*, 57.
Nable, A, Negm, M, & Zaki, F. (2008). Colloid surf a physicochem. *Eng Aspect, 322*, 97.
Naderi, E, Jafari, AH, Ehteshamzadeh, M, & Hosseini, MG. (2009). *Materials Chemistry and Physics, 115*, 852–858.
Noor, EA. (2009). *Materials Chemistry and Physics, 114*, 533–541.
Nyikos, L, & Pajkossy, T. (1985). *Electrochim Acta, 30*, 1533.
Obot, lB, & Obi-Egbedi, NO. (2010). *Corrosion Science, 52*, 657–660.
Oguzie, EE, Li, Y, & Wang, FH. (2007). *Journal of Colloid and Interface Science, 310*, 90.
Oguzie, EE, Enenebeaku, CK, Akalezi, CO, Okoro, SC, Ayuk, AA, & Ejike, EN. (2010). *Journal of Colloid and Interface Science, 349*, 283–297.
Popova, A, Sokolova, E, Raicheva, S, & Christov, M. (2003). *Corrosion Science, 45*, 33.
Qu, Q, Li, L, Bai, W, Jiang, S, & Ding, Z. (2009). *Corrosion Science, 51*, 2423–2428.
Quraishi, MA, & Sharma, HK. (2002). *Materials Chemistry and Physics, 78*, 18.
Schmitt, G. (1984). *British Corrosion Journal, 19*, 165–169.
Singh, DDN, Singh, TB, & Gaur, B. (1995). *Corrosion Science, 37*, 1005.
Solmaz, R, Kardaş, G, Ulha, MC, Yazlcl, B, & Erbil, M. (2008). *Electrochim Acta, 53*, 5941–5952.
Soltani, N, Behpour, M, Ghoreshi, S, & Naeimi, H. (2010). *Corrosion Science, 52*, 1351–1361.

Sorkhabi, HA, Shaabani, B, & Seifzadeh, D. (2005). *Electrochim. Acta, 50*, 3446.
Tian, BR, & Cheng, YF. (2008). *Corrosion Science, 50*, 773–779.
Umoren, SA, & Open, Journal (2009). *Corrosion, 2*, 175–188.
Umoren, SA, Li, Y, & Wang, FH. (2010). *Corrosion Science, 52*, 2422–2429.
Vračar, LM, & Dražić, DM. (2002). *Corrosion Science, 44*, 1669.
Wang, L. (2001). *Corrosion Science, 43*, 2281–2289.
Yan, Y, Li, W, Cai, I, & Hou, B. (2008). *Electrochim Acta, 53*, 5953.

doi:10.1186/s40712-014-0024-5
Cite this article as: Dinmohammadi *et al.*: Water-based acrylic copolymer as an environment-friendly corrosion inhibitor onto carbon steel in 1 M H_2SO_4 in static and dynamic conditions. *International Journal of Mechanical and Materials Engineering* 2014 **9**:24.